Mohammed J. Talab
Sahar N. Rashid

Departments of Physics,
College of Science,
University of Tikrit,
Tikrit, IRAQ

Synthesis and Characterization of Ni@Co and Co@Ni Core-Shell Nanoparticles via Laser Ablation

This work aimed to study the synthesis and characterization of nickel (Ni) and cobalt (Co) nanoparticles, as well as (Co@Ni) and (Ni@Co) core-shell nanoparticles. Pulsed laser ablation in liquid (PLAL) technique using Nd:YAG laser at wavelength (1064 nm) was used in the synthesis in deionized water, and important structural and optical characterization techniques were used to characterize them. The results showed superior optical and structural properties of the core-shell nanoparticles compared to those synthesized individually, as their optical properties are more stable with larger energy gap values, where it has smaller crystal sizes, and their morphological analysis shows that they are more regular and have smaller average diameters. The results also showed the formation of metal oxide nanoparticles in all the prepared colloidal nanoparticles.

***Keywords*:** Colloidal NPs; Core-shell structure; Pulsed laser ablation; Metallic NPs
Received: 01 January 2025; **Revised:** 06 February 2025; **Accepted:** 13 February 2025

1. Introduction

The pulsed laser ablation in liquid (PLAL) is an efficient, modern, environmentally friendly, and pollutant-free technique for preparing colloidal nanoparticles (NPs) through rapid ablated a material target in a liquid medium. It is an interesting method for producing pure and stable nanoparticles, playing a significant role in a wide range of applications in various fields [1-3]. In general, laser material treatment is considered one of the important biological and industrial processes. The absorption of the laser beam by the materials affects the temperature distribution inside these materials, causing thermal stresses [4-7]. Research has shown that by modifying several factors, such as laser energy, pulse duration, repetition rate, wavelength, ablation time, and liquid level above the target material, the characteristics of the prepared nanoparticles can be influenced, as evident from their structural and optical characterized [8-10]. Recently, scientists and researchers have focused on synthesizing nanoparticles from various elements at the nanoscale, successfully developing a new type of composite nanoparticles, called core-shell, which consists of two or more individual nanomaterials [11-13]. These composite nanoparticles exhibit unique and novel physical and chemical properties, such as optical, electrical, thermal, and catalytic characteristics, combining the features of different materials from which they formed, in addition to the advantage of the effect of reducing the ratio of volume to surface area. This advancement accelerates the development of various applications [14-17]. Among the metal nanoparticles synthesized are CoNPs and NiNPs. These nanoparticles are notable for their ease of preparation and non-toxic nature when prepared individually.

Furthermore, core-shell nanoparticles are manufactured as nanocomposites with unique properties. Core@shell nanoparticles are a class of biphasic materials that consist of an inner core of one material and an outer shell of another material, resulting in structures of different natures. The choice of materials depends on the intended application. The unique properties of these composites are due to their various shapes, such as spherical, rosette, cubic, rod-shaped, etc. [17-19].

In this work, nanoparticles were synthesized using the PLAL technique for NiNPs and CoNPs. Subsequently, (Co@Ni) and (Ni@Co) NPs were synthesized. This technique is distinguished by its ability to produce metallic nanoparticles from a wide range of materials, which is allowing to compare the properties studied in this work.

2. Experimental Part

Cobalt nanoparticles and nickel nanoparticles were synthesized as colloidal nanoparticles by ablation of pure cobalt metal sheet and pure nickel metal sheet, respectively, in 7.5 ml of deionized water by exposing them to 1.064nm Nd:YAG laser with energy of 250 mJ, 1000 pulses, and repetition rate of 5 Hz. This process was carried out by placing the target metal sheet to be ablation in a glass beaker and immersing it in the liquid medium where the height of the liquid above the target was 7 mm and at a distance of 12 cm from the laser source, where both cobalt and nickel colloidal nanoparticles were prepared in this way. Then, the nanocomposite (Co@Ni) core-shell was prepared by placing the nickel sheet in the Co colloidal nanoparticles, in addition to preparing the nanocomposite (Ni@Co) core-shell by placing the cobalt sheet in the Ni colloidal nanoparticles. The synthesized samples were characterized structurally and optically using diagnostic techniques, namely x-ray diffraction (XRD), field-emission scanning electron microscopy (FE-SEM), energy-dispersive x-ray

spectroscopy (EDX), and ultraviolet-visible (UV-Vis) spectroscopy.

3. Results and Discussion

Figure (1) shows XRD patterns of colloidal nanoparticles solutions obtained using pulsed laser ablation. These patterns were compared with the standard JCPDS cards as in table (1). The presence of many prominent peaks in the XRD patterns confirmed that all synthesized nanoparticles were polycrystalline. Tow hexagonal close-packed (hcp) structures of CoNPs were observed. Also, two diffraction peaks in CoNPs conform to the face-centered cubic structure (f.c.c.) and two peaks of cubic cobalt oxide (Co_3O_4) nanoparticles. Crystallite size based on the dominant peak was 20.49 nm. The second diffraction pattern in this figure shows the formation of NiNPs in addition to NiONPs, where the diffraction peaks show an intensity consistent with a tectonic agglomerate structure of the f.c.c. phase, with a crystallite size of 22.27 nm. XRD pattern of Co@Ni nanoparticles confirms the formation of the cubic spinel phase of $NiCo_2O_4$ in addition to the f.c.c. of CoNPs and NiNPs where the dominance of the peaks belonging to the element cobalt (core) appears, with a crystallite size of 11.75 nm. XRD patterns of Ni@Co nanoparticles confirmed the formation of the cubic spinel phase of $NiCo_2O_4$, in addition to the f.c.c. phase of NiNPs, and the crystallite size of 10.54 nm, attributable to the effect of small particle size, with a clear dominance of the element nickel (core).

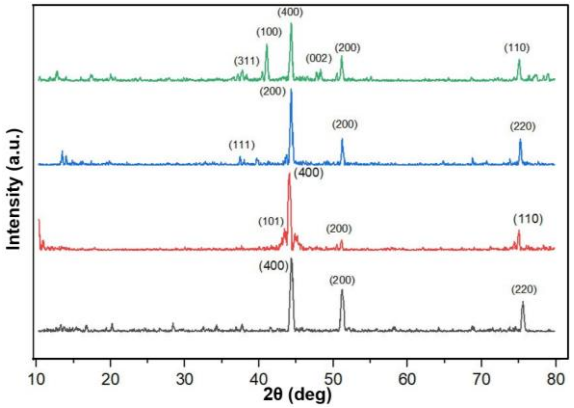

Fig. (1) XRD patterns of the synthesized nanoparticles

The peaks and other additional oxides are due to interactions between colloidal nanoparticles extracted and surrounding fluid, as differences in molecular pressures in the preparation environment caused by laser energy. From the diffraction profiles, it was observed that the Co@Ni nanoparticles core-shell peaks have lower broadness and intensity compared to CoNPs, which may be due to the presence of defects such as micro-stress caused by interstitial doping as well as dislocation density. Table (1) summarizes the results of XRD analysis and shows that the crystal sizes of nanoparticles, along with the diffraction angles, show a variety of values, which refers to the impact of metal mixing on the crystal structures. The average crystallite size (D) of NPs was calculated using Debye-Scherrer's equation [20,21]:

$$D = \frac{0.9\lambda}{\beta \cos\theta} \qquad (1)$$

where λ is the wavelength of the x-rays (1.54Å), θ is the diffraction angle, and β is the full width at half the maximum (FWHM) of the diffraction peak observed at the diffraction angle

In figures (2), (3), (4), and (5), the FE-SEM analysis of the synthesized samples was conducted to identify the surface morphology and nanoparticle size. In Fig. (2), CoNPs exhibit homogeneity with an average size of 20.72 nm. It is evident that the nanoparticles aggregate randomly, forming larger-sized particles. Figure (3) shows the morphology of NiNPs, where it is clear that clustering or overlapping of smaller particles leads to significant aggregation and the presence of some large particles. The image reveals an average nanoparticle size of 23.93 nm.

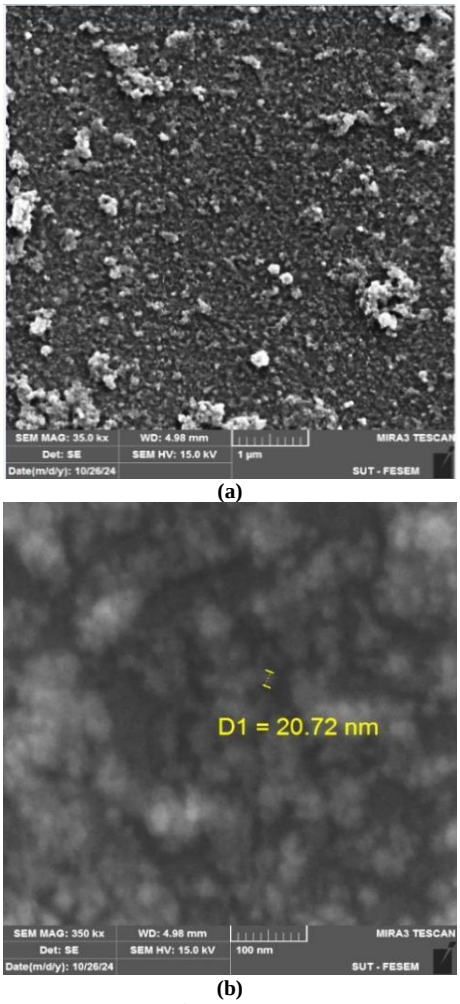

Fig. (2) FE-SEM images of synthesized CoNPs with scale of (a) 1µm, (b) 100nm

In figures (4) and (5), the quasi-spherical nanoparticles are shown with average sizes of 13.20 nm for (Co@Ni) nanoparticles and 15.25 nm for (Ni@Co) nanoparticles. The quasi-spherical nanoparticles display a distinctive core-shell structure variation. The lower average size indicates a more uniform and precise size distribution. The clustering and aggregation were mainly due to small dimensions, strong surface energy, and chemical bonds, this is consistent with [22].

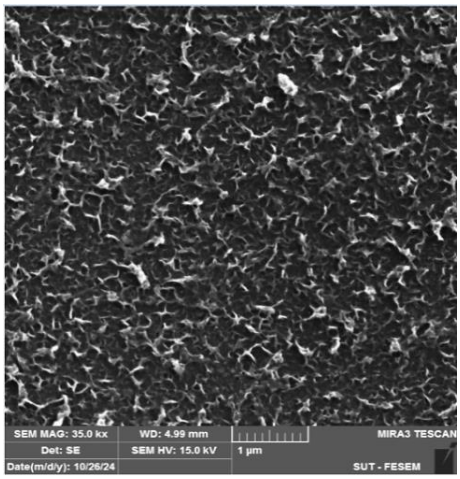

(a)

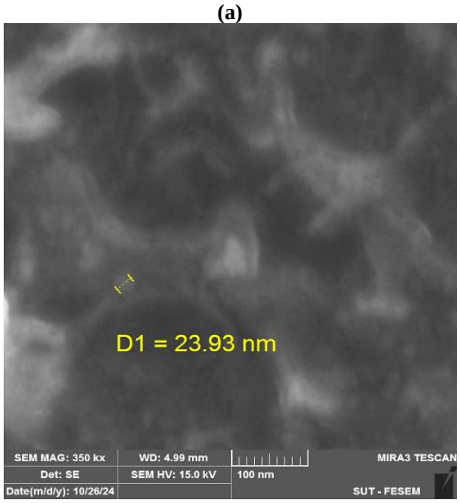

(b)

Fig. (3) FE-SEM images of synthesized NiNPs with scale of (a) 1µm, (b) 100nm

Through the typical EDX analysis of the prepared colloidal nanoparticles solutions, the elemental data and analyses in figures (6), (7), (8), and (9) indicate the presence of the prepared nanoparticles; CoNPs and NiNPs, along with their oxides, were the composition of the prepared materials appeared in the form of peaks. The source of oxygen is attributed to the surrounding environment, as the ablation process wasn't conducted in a vacuum. Additionally, the preparation medium, which is high-purity water, contains oxygen, as well as the surrounding environment of the EDX instrument itself.

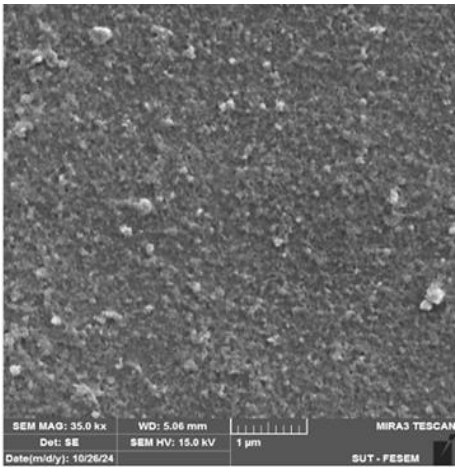

(a)

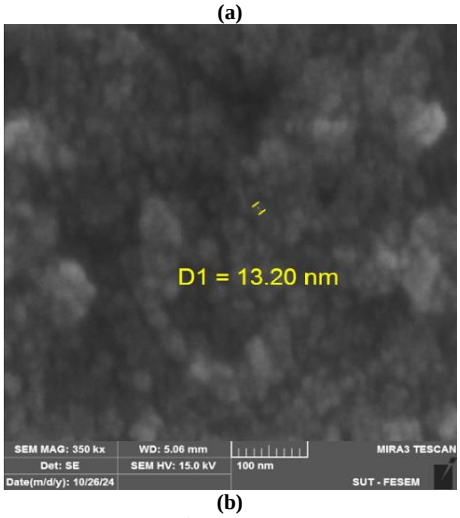

(b)

Fig. (4) FE-SEM images of synthesized (Co@Ni) nanoparticles with scale of (a) 1µm, (b) 100nm

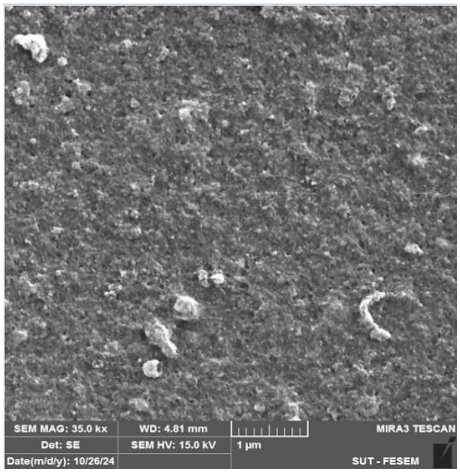

(a)

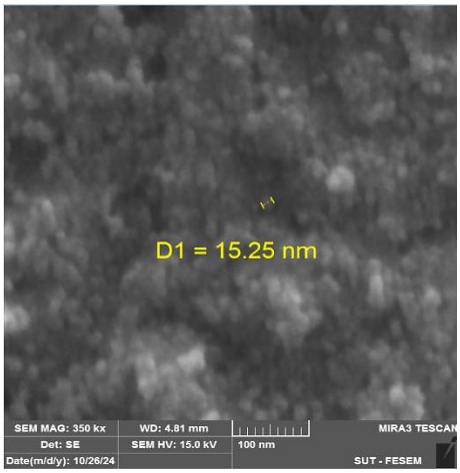

(b)

Fig. (5) FE-SEM images of synthesized (Ni@Co) nanoparticles with scale of (a) 1µm, (b) 100nm

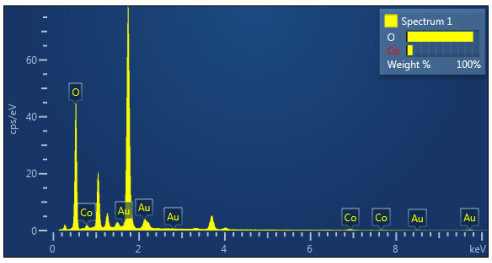

Fig. (6) EDX spectrum of CoNPs

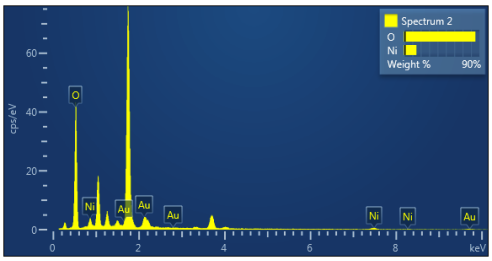

Fig. (7) EDX spectrum of NiNPs

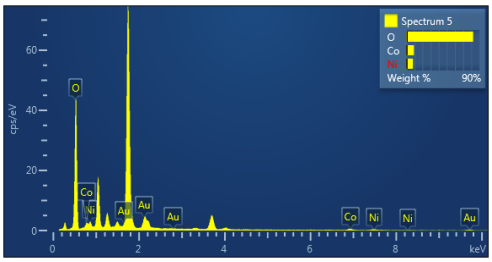

Fig. (8) EDX spectrum of (Co@Ni)NPs

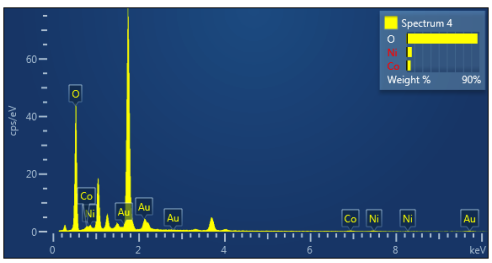

Fig. (9) EDX spectrum of (Ni@Co)NPs

Figure (10) represents the optical absorption spectrum, optical conductivity, and energy gap of CoNPs, NiNPs, (Co@Ni)NPs, and (Ni@Co)NPs suspended in deionized water, respectively. In Fig. (10a), the main peaks of the synthesized nanoparticles were observed, showing absorption was moderate when elements were mixed as a core-shell structure, along with distinct optical responses noted around the wavelength of 300 nm. CoNPs show the highest absorbance. The prominent peaks of the surface plasmon resonance (SPR) are higher in (Co@Ni)NPs and CoNPs, attributed to the more efficient distribution of these nanoparticles and increasing the nanoparticles concentration in the solution. In Fig. (10b), the optical conductivity of the prepared nanoparticles, calculated from the Eq. (2) [23], was found to be highest around the SPR region, and its curves appeared to be regular for the core-shell nanoparticles, based on the analysis of their structural properties.

$$\sigma = \frac{anc}{4\pi} \quad (2)$$

where a the absorption coefficient, c is the light velocity, n is the refractive index

Figure (10c) illustrates the values of energy gap (E_g), which were calculated using the Tauc's equation [24], to be 3.3, 3.65, 3.35, and 3.45 eV for CoNPs NiNPs, (Co@Ni)NPs, and (Ni@Co)NPs, respectively. This indicates that the composite core-shell nanoparticles have energy gap values between those of CoNPs and NiNPs, demonstrating the effect of core-shell hybridization on improving electronic properties at the wavelength applied to the prepared samples.

$$ahv = B\left(hv - E_g\right)^{\frac{1}{2}} \quad (3)$$

where B is a constant, hv is the photon energy, and E_g is energy gap

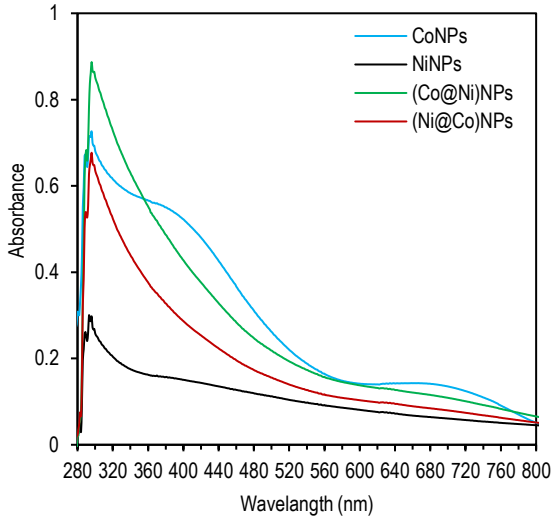

(a)

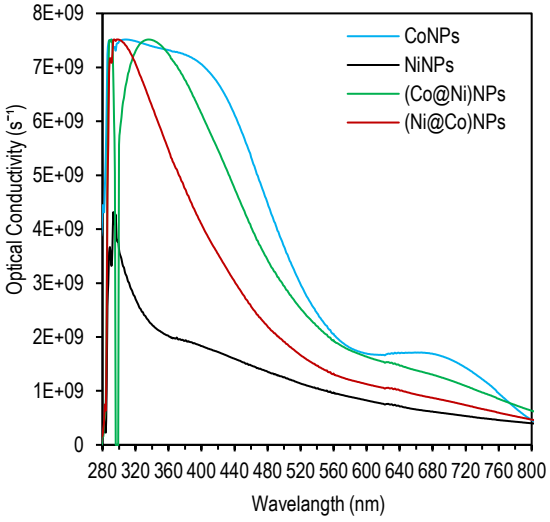

(b)

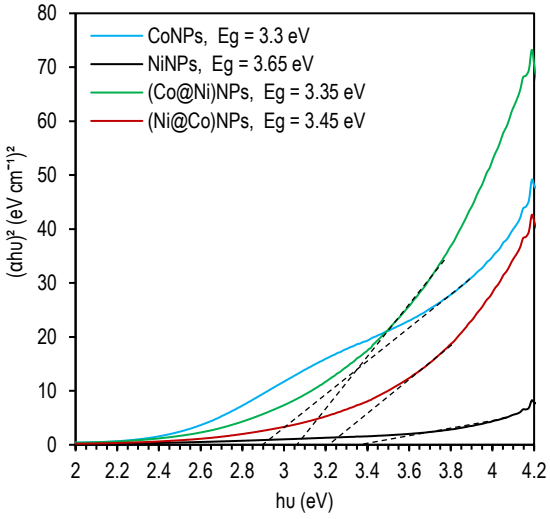

(c)

Fig. (10) UV-visible analysis of the synthesized nanoparticles (a) Absorbance, (b) Optical conductivity, (c) Energy gap

The results show that the energy gap values depend on the crystal size, as they increase with the decrease in the crystal size. In comparison, it was observed that the energy gap of CoNPs has a lower value than its values when the association occurs between Co and Ni nanoparticles, which have larger crystallite sizes. The same is true for the energy gap of NiNPs when compared to its values when this association occurs. The decrease in crystallite size leads to an increase in the energy gap value due to the quantum confinement phenomenon of energy levels. In other words, the distance between the valence bands and the conduction bands increases, so the energy gap increases. This result shows, under normal heat and light conditions, a higher relative stability of the prepared core-shell nanoparticles, as the material with a large energy gap needs more energy to interact and destabilize it.

4. Conclusion

Core-shell nanoparticles have significant potential in a variety of applications. (Co@Ni)NPs and (NI@CO)NPs were successfully synthesized using the PLAL technique, the cost-effective, fast, and environmentally friendly. The results show that the core-shell nanostructures composed of Co and Ni exhibit improved optical stability and morphology compared to single nanoparticles. The formation of nanocomposites of Co and Ni improved optical properties such as absorption and solution stability. These structures have the potential to contribute to the development of electronic, optical, biological, and environmental applications due to their enhanced properties. Understanding the synthesized mechanism of core-shell is crucial for controlling the properties of these nanoparticles.

References

[1] R.H. Ahmed, "Optical Properties of Iron Oxide Thin Films Prepared by Pulsed Laser Ablation Method", *Tikrit J. Pure Sci.*, 26(3) (2021) 84-88.

[2] E. Fazio et al., "Nanoparticles engineering by pulsed laser ablation in liquids: Concepts and applications", *Nanomater.*, 10(11) (2020) 2317.

[3] M.T. Twafeeq and A.M. Falah, "Ag/TiO_2 core/shell NPs synthesized by laser ablation and its antibacterial activity", *Tikrit J. Pure Sci.*, 26(6) (2021) 78-90.

[4] A.S. Jasim, K.A. Aadim and S.N. Rashid, "Optical and Structural Properties of Cobalt Nanoparticles Synthesized by Laser Ablation", *Iraqi J. Sci.*, 63(10) (2022) 4292-4304.

[5] M.M. Shehab and K.A. Aadim, "Spectroscopic diagnosis of the CdO: CoO plasma produced by Nd:YAG laser", *Iraqi J. Sci.*, 62(9) (2021) 2948-2955.

[6] A.S. Jasim, K.I. Mohammed and S.N. Rashid, "Effect of annealing by CO_2 laser on Structural and optical properties of zinc oxide thin films prepared by Sol–gel method", *Tikrit J. Pure Sci.*, 21(4) (2016) 112-121.

[7] A.N. Salih and U.I. Hassan, "Study the effect of the type and nature of the substrate on the optical properties of the thin films of (NiO) prepared by spin coating method", *Tikrit J. Pure Sci.*, 20(1) (2015) 126-131.

[8] R.H. Ahmed, A.E. Ibrahim and K.A. Aadim, "Effect of laser energy on grain size of cadmium oxide nanoparticles in ethanol by PLD method", *Tikrit J. Pure Sci.*, 23(7) (2018) 85-91.

[9] D. Zhang, Z. Li and K. Sugioka, "Laser ablation in liquids for nanomaterial synthesis: diversities of targets and liquids", *J. Phys.: Photon.*, 3(4) (2021) 042002.

[10] O.A. Hammadi, M.K. Khalaf and F.J. Kadhim, "Fabrication of UV Photodetector from Nickel Oxide Nanoparticles Deposited on Silicon

Substrate by Closed-Field Unbalanced Dual Magnetron Sputtering Techniques", Opt. Quantum Electron., 47(12) (2015) 3805-3813.
[11] K.K. Wan et al., "Introduction to nanomaterials. In Carbon Nanomaterials and their Composites as Adsorbents", *in Carbon Nanomaterials and their Composites as Adsorbents*, Springer, Cham. (2024) pp. 1-15.
[12] C. Cerezo-Navarrete et al., "Structural transformation of carbon-encapsulated core-shell CoNi nanoparticles during magnetically induced CO_2 reduction into CO", *Appl. Catal. B: Enviro. Ener.*, 347 (2024) 123780.
[13] O.A. Hammadi and N.E. Naji, "Fabrication and Characterization of Polycrystalline Nickel Cobaltite Nanostructures Prepared by Plasma Sputtering as Gas Sensor", Phot. Sen., 8(1) (2018) 43-47.
[14] M. Yang et al., "Zero→ two-dimensional metal nanostructures: an overview on methods of preparation, characterization, properties, and applications", *Nanomater.*, 11(8) (2021) 1895.
[15] B.M. Ghdhaib and S.N. Rashid, "Characterization of Nickel and Nickel Oxide Nanoparticles Prepared by Laser Ablation Technique: Effect of Laser Wavelength and Energy", *Iraqi J. Appl. Phys.*, 20(3) (2024) 477-484.
[16] E.N. Ghaem, D. Dorranian and A.H. Sari, "Characterization of cobalt oxide nanoparticles produced by laser ablation method: Effects of laser fluence", *Physica E: Low-dimen. Syst. Nanostruct.*, 115 (2020) 113670.
[17] X. Chen et al., "Synthesis and characterization of a $NiCo_2O_4$@$NiCo_2O_4$ hierarchical mesoporous nanoflake electrode for supercapacitor applications", *Nanomater.*, 10(7) (2020) 1292.
[18] E. Yang et al., "Coke resistant NiCo/CeO_2 catalysts for dry reforming of methane derived from core@shell Ni@Co nanoparticles", *Appl. Catal. B: Enviro.*, 339 (2023) 123152.
[19] C.F. Jones et al., "Conductive Core−Shell Nanoparticles: Synthesis and Applications", *The J. Phys. Chem.*, 128(27) (2024) 11083-11100.
[20] A. Monshi, M.R. Foroughi and M.R. Monshi. "Modified Scherrer equation to estimate more accurately nano-crystallite size using XRD", *World J. Nano Sci. Eng.*, 2(3) (2012) 154-160.
[21] L.E. Smart and E.A. Moore, **"Solid State Chemistry: An Introduction"**, Taylor & Francis, 3rd ed., (USA, 2005), Ch. 2, p. 105.
[22] K. Balakrishnan, G. Thangavel and N. Murugesan, "Structural, morphological, optical and electrochemical aspects of novel synthesized Nickel Oxide and Cobalt doped Nickel Oxide nanoparticlesâ An alternate electrode material for energy storage devices", *Int. J. Nano Dimen.*, 14(2) (2023) 191-202.
[23] E.D. Palik, **"Handbook of Optical Constants of Solids"**, Academic Press (USA, 1998), Ch. 2, p. 17.
[24] J. Singh, **"Optical Properties of Materials and Their Applications"**, John Wiley & Sons Inc. (USA, 2006), Ch. 3, p. 68.

Table (1) XRD analysis results of the synthesized nanoparticles

Sample	NPs	Phase	2θ (deg)	FWHM (rad)	D (nm)	(hkl)	JCPDS card no.
Co	Co_3O_4	cubic	37.74	0.375	22.3793	(311)	74-2120
	Co	hcp	41.04	0.486	17.44692	(100)	05-0727
	Co_3O_4	cubic	44.23	0.381	22.49822	(400)	74-2120
	Co	hcp	48.21	0.343	25.36395	(002)	05-0727
	Co	fcc	51.09	0.412	21.36305	(200)	15-0806
	Co	fcc	75.18	0.328	30.55411	(110)	15-0806
Ni	NiO	fcc	38.14	0.425	19.7701483	(111)	04-0835
	NiO	fcc	44.35	0.385	22.27397	(200)	04-0835
	Ni	fcc	51.17	0.253	34.80046	(200)	04-0850
	Ni	fcc	76.92	0.257	39.46093	(220)	04-0850
Co@Ni	Co	hcp	43.39	0.296	28.87363	(101)	05-0727
	$NiCo_2O_4$	cubic spinel	44.06	0.729	11.75126	(400)	20-0781
	Ni	fcc	51.18	0.258	34.12746	(200)	04-0850
	Co	fcc	75.2	0.215	46.61905	(110)	15-0806
Ni@Co	$NiCo_2O_4$	cubic spinel	44.36	0.813	10.54832	(400)	20-0781
	Ni	fcc	51.35	0.372	23.6859	(200)	04-0850
	Ni	fcc	75.03	0.421	23.78069	(220)	04-0850

